RESEARCH ARTICLE

Wireless Channel Characterization for UWB Communication in Capsule Endoscopy

KATJANA LADIC [1], **KAMRAN SAYRAFIAN** [2], (Senior Member, IEEE),
DINA ŠIMUNIĆ [1], (Senior Member, IEEE), AND
KAMYA YEKEH YAZDANDOOST [3], (Senior Member, IEEE)

[1]Faculty of Electrical Engineering and Computing, University of Zagreb, 10000 Zagreb, Croatia
[2]National Institute of Standards and Technology, Gaithersburg, MD 20899, USA
[3]Optical Access Network Laboratory, KDDI Research Inc., Fujimino, Saitama 356-8502, Japan

Corresponding author: Katjana Ladic (katjana.krhac@fer.hr)

ABSTRACT Since its invention in the early 1990s the technology behind capsule endoscopy has been making rapid progress. The emergence of high-resolution miniature video cameras along with other microsensor technology have increased the data rate and power consumption requirements for the next generation of these capsules. These requirements along with other advantages have made the Ultra-Wideband (UWB) technology an attractive candidate for wireless communication with the capsule endoscope. Our objective in this paper is to obtain a statistical pathloss model that effectively captures the impact of the transmitter antenna orientation and various body tissues as the capsule moves along its natural path inside the small intestine. To obtain this model, we have developed a 3D immersive platform including a detailed computational human body and gastrointestinal tract models that allow for an in-depth study of the wireless propagation channel between the capsule and the on-body receivers. Using the immersive platform, we have also developed an innovative methodology that enables judicious placement of the capsule along its natural trajectory inside the small intestine. Using this methodology, we obtain sufficient number of sample measurement points with a balanced transmitter-receiver distance distribution while covering the entire small intestine. The results show the significant impact of the orientation of the capsule antenna on the fading component of the statistical pathloss model. This knowledge is essential to better understand the feasible communication range of the capsule as it traverses the small intestine. Our research also provides further information on the time domain characteristics and multipath propagation for the UWB communication channel with a capsule endoscope. We show that the time domain channel responses typically consist of very few noticeable delayed paths. We also conjecture that the more feasible frequency range within the unlicensed UWB spectrum for communication with a capsule endoscope is 3.1 GHz to 4.1 GHz.

INDEX TERMS Capsule endoscopy, statistical pathloss model, ultra-wideband, frequency response, multipath propagation.

I. INTRODUCTION

Gastrointestinal (GI) endoscopy is a diagnostic and therapeutic procedure that enables doctors or clinicians to visually examine, image, assess, and treat illnesses in the upper digestive system. Endoscopy procedure plays a significant part in nearly all GI-related diseases as well as a crucial role in clinical research. It is estimated that more than 20 million GI endoscopies are performed each year in the United States [1].

In traditional upper GI endoscopy, a long, flexible tube equipped with an image sensor (camera) is passed through the patient's throat to reach the esophagus, stomach, and duodenum. Capsule Endoscopy (CE), on the other hand, uses an ingestible capsule equipped with a miniaturized wireless camera. The technology was invented in early 1990s by Gavriel Iddan and the first product became officially

available in 2001 [2]. CE provides a minimally invasive alternative imaging technology for the Gastrointestinal (GI) tract of the human body. CE is a painless, and effective diagnostic technology for various health disorders such as obscure gastrointestinal bleeding, tumors, cancer, as well as celiac and Crohn's diseases [3]. The breakthrough impact of CE in medicine is that it also allows the observation of abnormalities throughout the entire small intestine. The small intestine is the longest segment of the GI tract with a length of around 5 m to 7 m. The tubular structure inside the small intestine is not accessible by today's conventional wired endoscopy or colonoscopy [4], [5]. In addition, traditional endoscopy is often described as painful and uncomfortable for patients while CE can achieve the same objective without any discomfort.

While moving through the GI tract, the information captured by the embedded camera in the capsule is transmitted wirelessly to reach the receivers that are typically placed inside a belt worn by the patient. Commercially available capsule endoscopes mostly operate at Medical Implant Communication Service (MICS) frequency band (i.e., 402 MHz to 405 MHz). They provide images with a maximum resolution of 512×512 pixel and around 2 to 6 frames per second [6], [7]. Battery lifetime is often a limiting factor for the operation of these capsules as in 16.5% of procedures, the battery cannot support the entire journey of the capsule along the GI tract [8]. The next generation of endoscopy capsules are expected to deliver higher resolution images or even videos as well as more diagnosis and therapeutic functionality. This translates to higher data rates for the transmission of information from the capsule. The higher data rate requirement along with lower complexity of the transceiver make the Ultra-Wideband (UWB) technology an attractive candidate for wireless communication with the capsule. The unlicensed UWB spectrum (3.1 GHz to 10.6 GHz) is the frequency band currently being considered for the ingestible electronics and implants use-cases in the upcoming revision of the international standard for Body Area Networks (i.e., IEEE Std 802.15.6ma) [9]. A standard-based radio communication protocol for capsule endoscopes not only simplifies the development process of its transceivers but also supports interoperability among products from different manufacturers.

Using UWB technology within the 3.1 GHz to 10.6 GHz range can enable high data rate transmission from the capsule; and therefore, supports applications such as high-resolution video. However, high attenuation of the body tissues at these frequencies could create a challenge to establish a reliable communication link. The variety of organs and tissues with different frequency-dependent dielectric properties might also lead to further distortion in the transmission of a wideband signal. The communication channel between the capsule and an on-body receiver is also affected by the transmitter and receiver antennas. Although higher frequencies incur higher propagation loss through the human body tissues, they allow miniaturization of the

antennas used for this application. This is especially critical for the capsule where limitations on its physical size and shape create more stringent restrictions on the design of the transmitting antenna.

Understanding the radio frequency (RF) propagation channel in a wireless communication link is essential for efficient transceiver design. However, for implant or ingestible electronics, obtaining this knowledge is a challenging task. Performing in vivo experiments in a living human to conduct RF signal measurements is virtually impossible. Therefore, research in this area is typically done through simulations with computational models, experiments using animals or liquid phantoms [10], [11], [12], [13], [14], [15], [16], [17], [18].

A. LITERATURE REVIEW

In the past several years, there have been few studies in the literature focusing on UWB channel evaluation for capsule endoscopy application. In [11], authors used the finite difference time domain (FDTD) numerical method with an anatomical human body model to find the channel characteristics and investigate feasibility of space diversity to enhance UWB communication performance. Using five receiver locations on the abdomen, the pathloss exponents and standard deviation of the shadow fading were reported to range from 1.00 to 2.07, and 7.1 dB to 8.48 dB respectively. The resulting low pathloss exponents in [11] are likely due to several factors including the simple line element assumed for the capsule antenna, the limited variations of the distances used in the simulations and using free space antenna gains in the computation. Additionally, it was not specified whether the computational model used for the small intestine included sufficient details for the placement of the capsule antenna. The authors conclude by showing the possibility of using the UWB technology to achieve a data-rate of 80 Mbps for capsule endoscopy.

Authors in [12] developed an Impulse Radio UWB (IR-UWB) communication system for implant applications. They conducted experiments using a liquid phantom and a living animal to evaluate the performance of the system operating at 3.4 GHz to 4.8 GHz band. Measurements at five different distances between the transmitter and receiver antennas were conducted using a liquid phantom. At 4 GHz, the authors report a pathloss of around 80 dB at a distance of 7 cm. Five transmitter locations were also considered inside a pig to evaluate the communication with the receiver on the surface. Despite a pathloss of more than 80 dB, they concluded that their IR-UWB implant communication system could achieve a bit error rate of around 10^{-2} with a data rate of 1 Mb/s up to a distance of 12 cm between the capsule transmitter and the on-body receiver. Although, this study provides some information about the applicability of UWB for implants, their results don't necessarily apply to ingestible electronics applications such as CE. The complexity of the GI tract environment and possibility of various positions

and orientations for the transmitting antenna have not been considered in their evaluation.

In [13], authors analyze the pathloss, specific absorption rate (SAR), and temperature variation of the tissues inside the human body caused by an IR-UWB-based capsule endoscope inside the abdomen. Since their primary objective is the electromagnetic power absorption and thermal effects caused by in-body propagation of the wireless signal from the capsule, the pathloss calculation is more focused on in-body propagation channel. To characterize this channel, the authors used a voxel-based human body model and computed the pathloss based on time-varying Poynting vector at points that lie within the tissue medium between the capsule and the body surface. The resulting pathloss model for the in-body channel does not include the effect of the on-body receiver which is normally part of the CE communication channel. Based on their simulations, the authors state that pathloss at the surface of the body varies from 80 to 100 dB. However, they note the possible dependency of this value on the frequency as well as the position of the capsule inside the GI tract.

Authors in [14] developed an UWB antenna based on polarization diversity technique for implant applications. They evaluated the performance of the antenna through computer simulation, liquid phantom as well as experiment with a living animal. Considering the frequency range 3.4 GHz to 4.8 GHz, the authors report the average pathloss between the implant and on-body antennas with distances ranging from 2 cm to 12 cm. Based on the measurement data from 6 sample points inside a liquid phantom and 8 sample points inside a pig, they conclude that using polarization diversity for the implant antenna can improve the performance of the UWB communication link. In [15] and [16], authors present a comparative pathloss study for capsule endoscopy in the frequency range 3.1 GHz to 5.1 GHz. Simulations using a simple computational model, liquid phantom experiment and in vivo measurements with a living porcine were conducted to do the study. A distance range of approximately 3 cm to 8 cm was considered for evaluation of the pathloss between the capsule antenna and the on-body receiver. The 8 cm limitation on distance is primarily due to the noise floor of the vector network analyzer used for signal measurements. For a logarithmic pathloss model, the pathloss exponents and standard deviations of the shadowing component were reported to range from 5.3 dB to 10.3 dB, and 3.6 dB to 28.1 dB across simulations, liquid phantom, and in vivo measurements, respectively.

In [17] and [18], authors studied the propagation channel between the capsule antenna and a directional on-body antenna using a voxel-based computational body model for the frequency range 3.75 GHz to 4.25 GHz. Three capsule locations inside the small intestine and two on-body locations were considered for their evaluation. The authors concluded that the channel characteristics strongly depend on the locations of the antennas inside the small intestine and on the abdomen surface. In addition, they showed that the antenna

radiation pattern and capsule orientation have a strong impact on the received signal strength. The extended version of their study covering both small and large intestines are available in [19] and [20]. A study on the impact of breathing on the received power from UWB implanted devices has also been carried by the authors in [21]. Their results show that both the relative received power and its phase exhibit an oscillatory process with time which can be modeled by an absolute value of a cosine function.

B. RESEARCH OBJECTIVES

From the limited number of studies on this topic in the literature, it can be observed that using different anatomical or computational body models, simulation or experiment scenarios and capsule or on-body antennas often lead to noticeable variations in the resulting statistical channel models for capsule endoscopy. As common in almost all in-body or on-body propagation studies, the transmitter and receiver antenna characteristics will become part of the propagation channel. This is due to the near field coupling of the antenna and the surrounding non-homogenous tissues with frequency dependent complex conductivity in the human body [22]. For this reason, using realistic and practical antennas for propagation study in these applications becomes important. Each application or use-case could necessitate a different type of antenna, and measurement (or simulation) scenarios. For these reasons, the authors believe that channel models for ingestible applications such as CE may not necessarily be the same as implant applications operating at UWB frequencies. For capsule endoscopy, the size of the transmitting antennas used in some of the studies in the literature is larger than the current commercially available capsules (i.e., 11 mm × 26 mm). The antenna size could impact the realized gain and efficiency of the antenna, which in turn affects the resulting pathloss. Therefore, it will be more accurate to use antennas with practical sizes during the virtual or physical measurements. In addition, different antenna orientations are typically not considered as part of the simulation or physical experiment scenarios to measure the pathloss. The orientation of the capsule antenna continually changes with respect to the on-body receiver as the capsule traverses the complex path along the GI tract. This is especially the case for the small intestine. Due to its non-isotropic radiation pattern, the antenna orientation may have a substantial impact on the experienced pathloss. Therefore, this impact should be captured in a practical statistical pathloss model for this application.

To obtain pathloss information, liquid phantom body models are sometimes used by researchers to conduct physical measurements. A liquid phantom can mimic a single (or multi-) layer dielectric environment. The material at each layer homogeneously models the dielectric properties of a specific tissue. However, the human body is a non-homogenous complex environment with multiple tissues having a wide range of frequency-dependent dielectric

properties. For wireless implant applications where the locations of the stationary pair of implant and on-body receiver is known, a reasonably matching multi-layer liquid phantom can be designed to better represent the environment between the implant transmitter and the on-body receiver. For CE applications, on the other hand, the RF signal transmitted by capsule antenna could experience different composition of body tissues or organs before it reaches the on-body receiver as the capsule moves along the GI tract. For this reason, discrepancies are usually observed between the pathloss results obtained by using liquid phantoms and the limited experiments with living animals.

Experiment with living animals is extremely challenging. Due to obvious anatomical or surgical limitations, very few antenna positions can be considered inside the animal's small intestine, leading to a small number of measurement samples. Radio signal leakage from the capsule antenna through the connecting cables and possible errors in the estimated distance between the capsule and on-body antennas during pathloss measurements are among other challenges in doing in vivo experiments.

Compared to liquid phantoms, computational body models can better approximate the non-homogeneous and diverse dielectric environment in CE application to conduct propagation studies. However, the complexity and required computational resources to use such models significantly increase with their level of details and resolution. To lower the complexity of the simulations and achieve manageable runtime, most of the studies in literature use a partial computational body model (e.g., abdominal area) with simplified and reduced number of body organs. This simplification impacts the ability to define more accurate scenarios for capsule placement inside the desired segment of the GI tract. For example, having a model that includes the tubular structure and internal surfaces of the digestive tract will be useful to identify the continuous path that the capsule travels through. Identification of this path will help to better define capsule antenna positions for conducting channel measurements.

In this paper, we have developed:

(a) An innovative three-dimensional (3D) immersive system including a sufficiently detailed computational human body model and validated antennas with practical dimensions to effectively emulate the UWB propagation from the capsule inside the small intestine.

(b) A methodology to identify appropriate capsule antenna positions along its natural path through the small intestine for virtual measurements. This methodology results in sufficient number of sample measurement points with a balanced transmitter-receiver distance distribution. This is generally required for proper derivation of a statistical pathloss model in wireless communication; however, it is not easily attainable in this application due to the spatial constraints in the capsule location inside the GI tract and the limited communication range with an on-body receiver.

(c) A statistical pathloss model that more effectively captures the impact of the capsule orientation in the fading component. To partially validate the accuracy of the results obtained by using this platform, we have also replicated a liquid phantom experiment and compared the resulting pathloss exponent obtained through physical and virtual measurements.

Our research also provides:

(d) Further information on the time domain characteristics and multipath propagation for the UWB communication channel with a capsule endoscope. We show that the time domain channel responses typically consist of very few noticeable delayed paths. We also conjecture that the more feasible frequency range within the unlicensed UWB spectrum for communication with a capsule endoscope is 3.1 GHz to 4.1 GHz.

The rest of this paper is organized as follows. Section II presents the 3D immersive system that has been developed to conduct virtual measurements. Antennas used in our experiments are described in Section III. The methodology to select simulation scenarios for channel measurements is explained in Section IV. Statistical pathloss modeling and channel characterization are discussed in Sections V and VI, respectively. Finally, conclusions and future work are described in Section VII.

II. 3D IMMERSIVE SYSTEM

A novel 3D immersive system to emulate RF propagation between a capsule endoscope and several on-body antennas has been developed at the Information Technology Laboratory of the National Institute of Standards & Technology (NIST) [10], [23], [24]. The system includes a 3D high resolution human body model with high-resolution GI tract model, a propagation engine (i.e., a full-wave electromagnetic field simulator (ANSYS HFSS[1])), validated models of the capsule and on-body antennas, and a 3D immersive & visualization platform (see Fig. 1). The electromagnetic simulation engine in this system enables the user to calculate a variety of different electromagnetic quantities; examples of which are scattering parameters, electric field, Poynting vectors, Specific Absorption Rate (SAR), etc.

The 3D computational body model used in this system has a resolution of 2 mm and includes frequency-dependent dielectric properties of 300+ parts of a male human body. These dielectric properties are user-definable in case custom modifications or changes are desired. To study propagation from a CE, a high-resolution 3D GI tract model without self-intersections or other non-manifold features has been developed and integrated with the 3D body model (see Fig. 2). Lack of self-intersections in the 3D model ensures

---

[1]Certain equipment, instruments, software, products, or materials are identified in this paper in order to specify the experimental procedure adequately. Such identification is not intended to imply recommendation or endorsement of any product or service by NIST, nor is it intended to imply that the materials or equipment identified are necessarily the best available for the purpose.
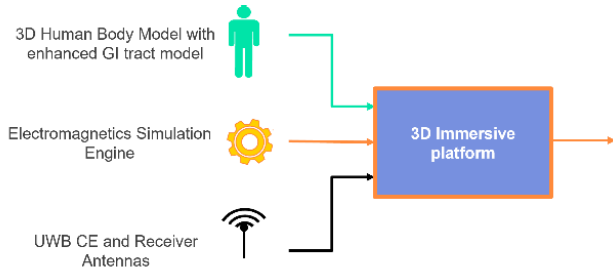
FIGURE 1. Immersive system used for CE propagation study.

that the inner and outer surfaces do not overlap or occupy the same space. Validated models of practical antennas have also been incorporated in the computational system to accurately characterize the wireless link between the capsule and the on-body receivers.
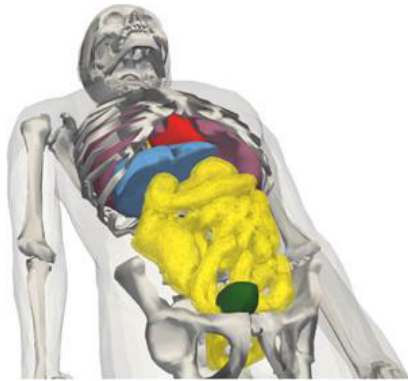

FIGURE 2. The 3D human body model with enhanced GI tract.

The 3D immersive platform assists a user to visualize and interact with the data as will be described in Section IV. The platform includes a visual display consisting of three large screens, stereoscopic glasses that are motion-tracked, and an input device that is also motion-tracked. The three large video projection screens are used as a single 3D stereo display. The 3D scene is updated for the position of the stereo glasses given by the motion tracker. This enables the immersive platform to present a virtual 3D world within which the user can move and interact with a virtual object. The virtual object in this study is the 3D human body model as observed in Fig. 3. This immersive system sufficiently captures the complexity of the propagation environment surrounding the capsule traveling through the GI tract; and therefore, has been used to study the UWB channel characteristics for capsule endoscopy.

III. ANTENNAS
Design of the proper antennas is one of the challenging tasks for wireless implants, ingestible electronics, and wearable sensors. The inhomogeneous environment surrounding these antennas makes the design more complicated compared to antennas intended for use in free space. Knowledge of the body organs and tissues in the vicinity of the antenna and
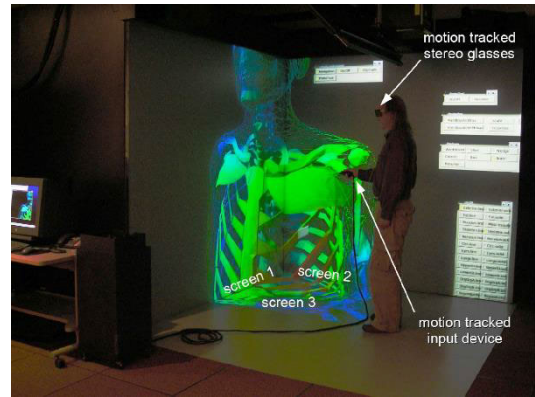

FIGURE 3. NIST immersive visualization platform [24].

information about the dielectric properties of those tissues at the target frequency and temperature are essential to achieve a good performance. Also, since de-embedding of the antenna gain pattern from the communication channel becomes impossible for in-body or on-body applications, using a realistic and practical antenna for channel characterization becomes extremely important. In the following subsections, we described the capsule and the on-body antennas that have been used along with our enhanced computational body model to accurately characterize the propagation channel.

A. CAPSULE ANTENNA
The capsule antenna is a single metallic layer planar antenna, printed on a Rogers1 RT Duroid 6100 (tm) substrate with dielectric constant of 10.2 and thickness of 0.8 mm. The antenna dimensions are 8.4 mm × 6 mm × 1.036 mm (see Fig. 4). These dimensions allow the antenna to practically fit inside typical CE pills that are available in the market. The diameter and length of the current commercially available pills are approximately 11 mm and 26 mm, respectively [25]. This antenna has been designed for UWB transmission from 3.1 GHz to 10.6 GHz using a layered tissue model [26].
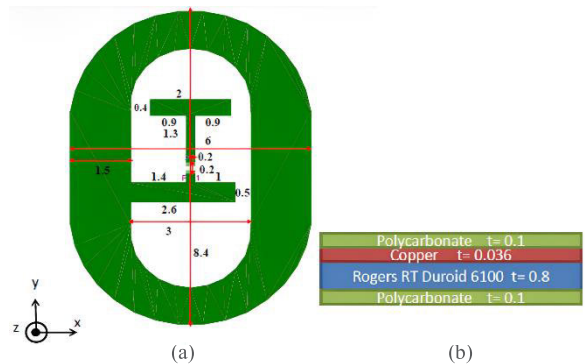

FIGURE 4. Configuration and dimension (in mm) of the CE antenna a) top view b) side view [26].

To ensure applicability of the antenna throughout the entire GI tract i.e., stomach, small and large intestines, three scenarios, using three separate layered tissue models,
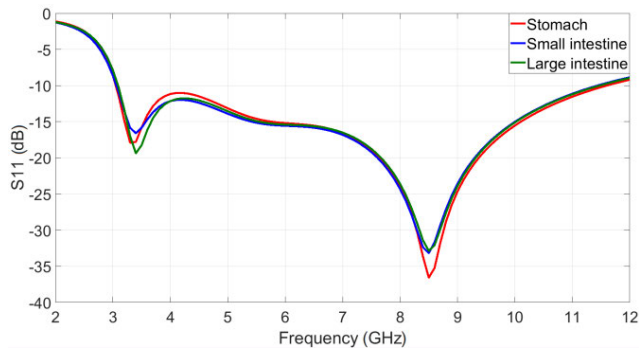
FIGURE 5. Reflection coefficient (S_{11}) of the capsule UWB antenna using customized layered tissue models for stomach (red), small intestine (blue) and large intestine (green).

FIGURE 7. In-body radiation pattern of the capsule antenna at 3.6 GHz.

were considered. The layers represent the tissues that will be surrounding the capsule antenna e.g., intestine, muscle, fat, and skin. The return-loss or equivalently the reflection coefficient (S_{11}) of the antenna for all three environments is shown in Figure 5. These results show the effectiveness of the antenna as the capsule travels through the entire GI tract.

To better investigate the influence of the inhomogeneous environment surrounding the antenna, the reflection coefficient of the antenna was also evaluated inside the stomach, small and large intestines of our computational human body model. The results shown in Fig. 6 indicate close agreement with the S_{11} obtained by using the simplified layered tissue models (i.e., Fig. 5).

FIGURE 6. Reflection coefficient (S_{11}) of the capsule UWB antenna inside the GI tract of the computational human body model: stomach (red), small intestine (blue), and large intestine (green).

Assuming that the capsule is inside the small intestine, an example of the 3D radiation pattern of this antenna at 3.6 GHz is shown in Fig. 7. As observed, the antenna orientation could make a significant impact on the propagation channel. Details of the antenna placement inside the small intestine is discussed in the next section.

B. ON-BODY ANTENNA

The on-body antenna in our study is a L-loop antenna that has been designed to operate in the lower UWB frequency range (i.e., 3.1 GHz to 5.1 GHz) [27]. As shown in Fig. 8, the dimensions of the on-body antenna are 24 mm ×
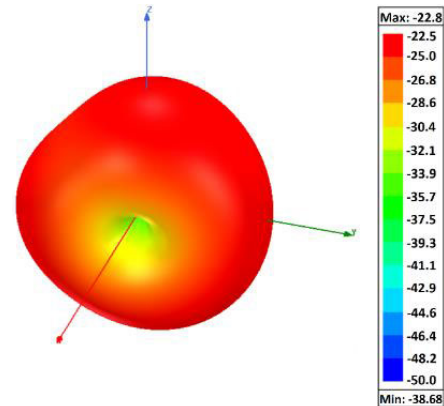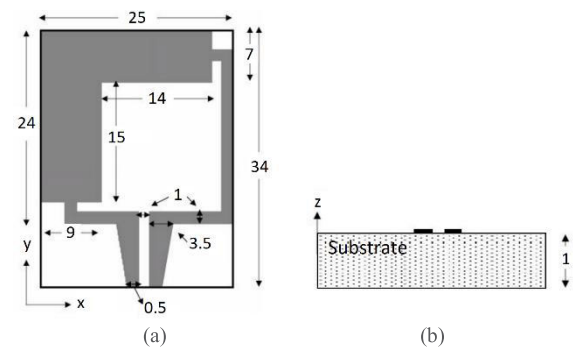

FIGURE 8. Configuration and dimensions (in mm) of the UWB L-loop on-body antenna a) top view, b) side view [28].

25 mm × 1 mm. To minimize the effect of the human body on the antenna characteristics, a RH-5 dielectric substrate with a thickness of 14 mm has been used to separate the antenna elements from the skin. Performance evaluation of the antenna showed that a separation of less than 14 mm could lead to a lower antenna gain, frequency shift and degradation of S_{11}. The relative permittivity of RH-5 is identical to air. This substrate will not affect the antenna parameters and the same level of Voltage Standing Wave Ratio (VSWR) as in free space can be achieved when the antenna is placed on the body surface near the abdomen.
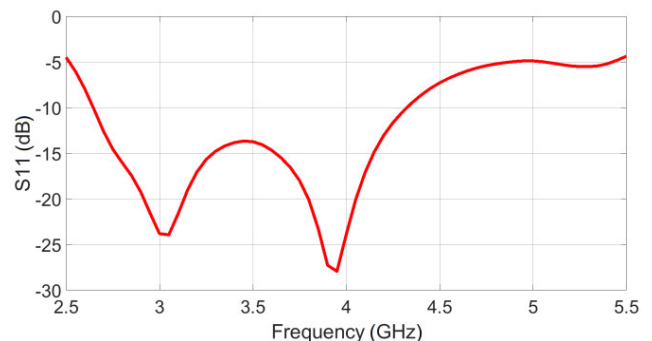

FIGURE 9. Reflection coefficient (S_{11}) of the on-body antenna with the computational body model.

The on-body antenna was also evaluated with the computational body model. The S_{11} of the antenna, shown in Fig. 9, is obtained by placing it on the abdomen area of the body model. As observed, the antenna shows good performance for the frequency range 3.1 GHz to 4.1 GHz.

Compared to the layered tissue model which the antenna was designed with, a slight frequency shift in VSWR was observed. However, such minor discrepancies can be expected as on-body antennas are usually sensitive to their exact distance from the body surface. The curvature on the computational body model surface causes some antenna distance deviation compared to the simple layered tissue model that was used during the design process. However, for the frequency range 3.1 GHz to 4.1 GHz, all antenna placements on the body surface covering the abdomen exhibited very good reflection coefficient.

As will be discussed later in this article, the attenuation of the RF signal transmitted from the capsule is very high for frequencies above 4.1 GHz. In other words, the bulk of the transmitted power that is received by the on-body sensor is concentrated within 3.1 GHz to 4.1 GHz. For this reason, we only consider this frequency range to study the UWB propagation channel in capsule endoscopy.

IV. DESIGN OF THE SIMULATION SCENARIOS USING THE IMMERSIVE PLATFORM

During the Capsule Endoscopy procedure, a patient typically wears a belt which includes multiple embedded receivers across the abdomen. In our study, positions of the receivers covering the abdomen area were approximately selected based on the sensor's locations used in the small bowel Pill-Cam Endoscopy procedure [29]. The blue squares in Fig. 10 show the locations of the on-body antennas during virtual experiments. We used a total of 10 receivers sufficiently apart from each other and spread across the abdomen surface. With these receivers, each capsule antenna location results in 10 independent propagation channels.
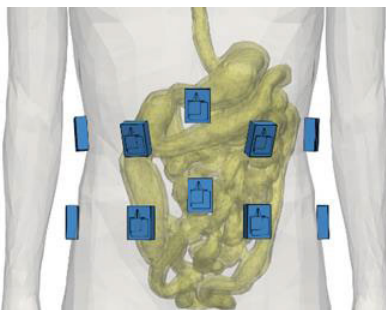

FIGURE 10. Locations of the on-body receivers (blue squares) covering the abdomen.

To place the capsule antenna inside the small intestine, we have first calculated the centerline that passes through the small intestine. This centerline (shown by the red color in Fig. 11) is the median of all possible paths that goes through the small intestine. On average, this line can be considered as
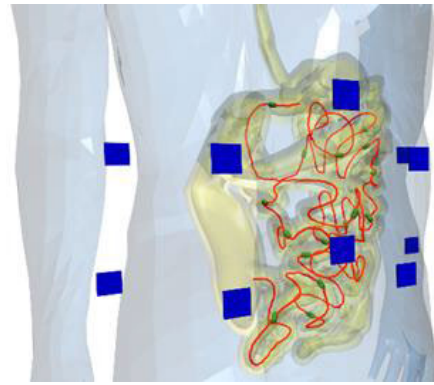

FIGURE 11. Locations of the on-body receivers (blue squares) and the centerline passing through the small intestine (red line).

the forward progression path of the capsule. Several sample antenna positions on this line should be selected to conduct electromagnetic simulations and obtain channel parameters for modeling purposes.

Using a high-performance computing server with 64 cores and 4 TB of highspeed memory, conducting a simulation to obtain the forward transmission coefficient of the channel (for each sample capsule antenna position) could take from 12 hours to 24 hours. This assumes a 20 MHz step size for the frequency range 3.1 GHz to 4.1 GHz. Although, some simplifications can be applied to the high-resolution computational body model to speed up these simulations (e.g., using only the torso and eliminating some of the less impactful organs such as blood vessels), judicious selection of the best candidate locations for the capsule antenna inside the small intestine is necessary in order to keep the total simulation runtime manageable and have a balanced transmitter-receiver distance distribution to derive a statistical pathloss model.

A. CAPSULE POSITION SELECTION USING AN INTERACTIVE TOOL AT THE IMMERSIVE PLATFORM

To obtain a statistical pathloss model for the communication link between the capsule and on-body receivers, a set of sample capsule positions inside the small intestine is needed. These capsule positions will define a set of simulation scenarios for radio wave propagation and channel measurements. The simple approach that comes to mind is to choose uniformly spaced locations along the tract centerline as sample positions. However, since the GI tract is a complex and intertwined path, uniformly spaced sample positions lead to scenarios where the capsule distances from the on-body receivers are heavily concentrated within certain ranges; and at the same time, there are not enough sample representatives in other distance ranges. This situation will negatively impact the accuracy of the statistical analysis needed for modeling the pathloss. The significance of a judicious selection of measurement points for statistical modeling has been shown in [30] using a simple liquid phantom model.

While it is conceivable to formulate a complicated mathematical approach to solve for the capsule location problem, the methodology described in the following subsection uses the immersive platform and offers a visually attractive and relatively easy alternative to find the desired set of locations. These locations must cover the entire area of the small intestine to comprehensively reflect the various wireless channels throughout the capsule journey. In addition, it is desired to have sufficient and almost uniformly distributed measurement samples for the entire range of interest in the transmitter-receiver separation. These conditions will ensure full representation of the small intestine environment and more accurate parameters in the resulting statistical pathloss model. Figure 12 shows a pseudo-transparent inner GI and body shell along with an example set of capsule positions. Capsules (shown in green) are placed and oriented along the centerline of the small intestine to better reflect the impact of the radiation pattern of the transmitting antenna on the pathloss measurement. d_1, d_2, d_3 are examples of the distance of one sample capsule position to three on-body receivers.
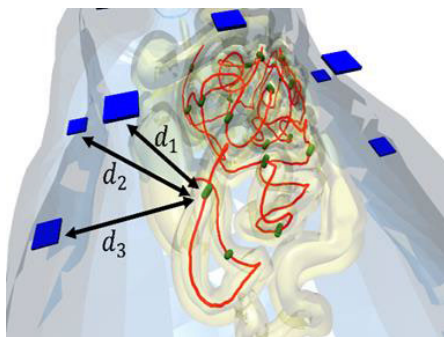

FIGURE 12. Sample capsule position along the small intestine centerline and its distance from the on-body receivers.

To select the best sample locations for the capsule antenna inside the small intestine (satisfying the conditions mentioned above), an interactive tool in the NIST immersive platform has been developed. The tool consists of several different modules with the following functions.

1) INITIAL POSITION SELECTION
To initiate the selection process, we first compute positions along the small intestine centerline that are at specific distances from the on-body receivers. The distances were chosen to be from 5 cm to 25 cm away from a receiver in increments of 2 cm.

2) SELECTING POSITIONS ALONG THE CENTERLINE
The immersive platform supports interactive probing and picking in a 3D scene. Using this capability, the user is also allowed to select positions along the small intestine centerline. However, we need to ensure that the position chosen has a specific distance to the receivers based on the precomputed positions in step 1. Thus, we implemented a K-nearest-neighbor search using geometric algorithms in the

Computational Geometry Algorithms Library (CGAL) [31] that takes the user-chosen position and then finds the closest matching precomputed position.

3) HISTOGRAM OF DISTANCES
To ensure that the user-selected positions are uniformly distributed across the range of interest (i.e., 5 cm to 25 cm), a histogram of distances between the on-body antennas and all the selected capsule locations is automatically generated (see Fig. 13). In this way, we can instantly see if the selected sample positions maintain the desired distribution and if further adjustments (i.e., sample position addition or subtraction) are needed. We continued this process to prudently select the final set of capsule locations required for pathloss measurement and modeling.
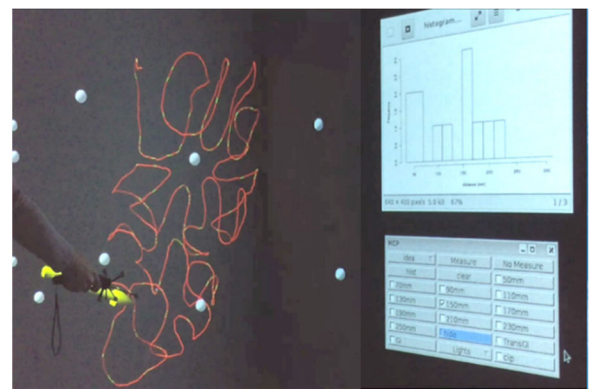

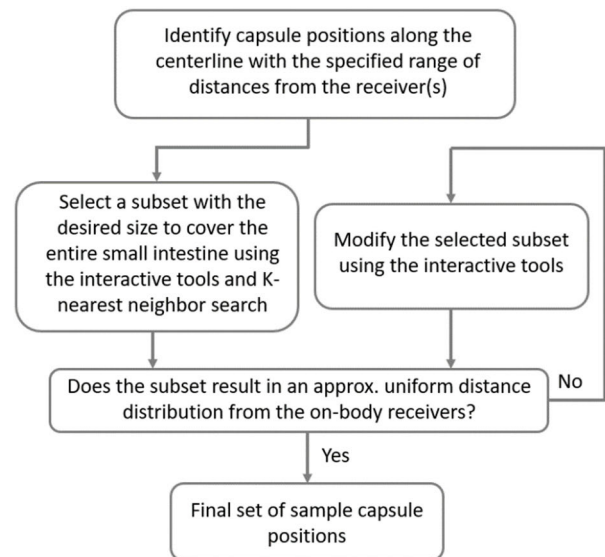FIGURE 13. Interactive tool inside the NIST 3D immersive platform.

FIGURE 14. Block diagram of the process to select the final capsule positions.

Following the above procedure and interaction with the 3D model of the GI tract inside the immersive platform, we carefully selected 20 candidate positions for the capsule antenna placement. This procedure has been summarized

in the block diagram shown in Fig. 14. The final set of transmitter positions resulted in an almost uniform distance distribution from all ten on-body receivers located on the abdomen surface.

V. STATISTICAL PATHLOSS MODELING

For each capsule position determined through the process described in the previous section, the forward transmission coefficients (S_{21}) of the wireless channel between the transmitter and each on-body receiver is computed for the frequency range 3.1 GHz to 4.1 GHz. ANSYS 3D high frequency simulation software has been used for this calculation with a frequency step size of 20 MHz. At any distance d, S_{21} represents the pathloss between the transmitter-receiver pair.

Define $PL(d, f)$ to be the pathloss in dB between the capsule antenna and an on-body receiver at distance $d \geq d_0$ and frequency $f \epsilon$ [3.14.1] GHz. Given the data from the selected measurement scenarios, the following log-distance statistical pathloss model is used to represent the capsule endoscope propagation channel:

$$PL(d, f) = PL(d_0, f) + 10n(f) \log_{10}\left(\frac{d}{d_0}\right) + S(f) \, d \geq d_0$$

(1)

where d_0 is the reference distance (here chosen to be 5 cm), $n(f)$ is the pathloss exponent at frequency f and $S(f)$ is the fading component at frequency f, modeling the deviation from the mean value due to different body tissues in the propagation path of the transmitted signal (e.g., bone, muscle, fat, etc.), receiver and transmitter positions and orientations and their antenna gains in different directions.

The pathloss exponent $n(f)$ heavily depends on the environment where the RF signal is propagating through. In free space, this exponent is two regardless of the frequency. However, since the human body is an extremely lossy environment, a higher value for this exponent is normally expected for propagation from wireless implants and ingestible electronics.
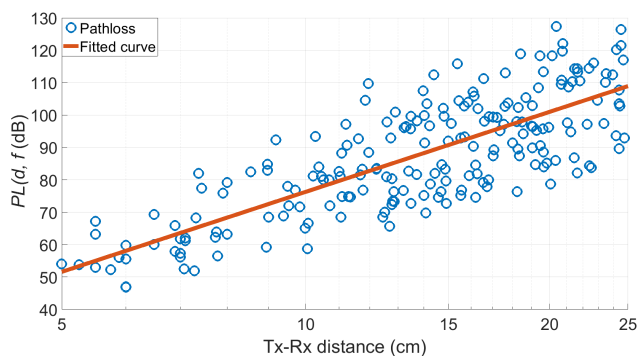
FIGURE 15. Scatter plot of the pathloss for the measured scenarios and the regression line at 3.6 GHz.

Figure 15 shows the scatter plot of the pathloss for the measurement scenarios (i.e., 200 propagation channels

resulting from 20 selected capsule positions and 10 on-body receivers) as a function of transmitter-receiver distance at 3.6 GHz frequency. The candidate capsule locations inside the small intestine covers a range of 5 cm to 25 cm distances from the on-body receivers. The solid line in red color is obtained by using the least squares linear regression and minimizing the root mean square deviation of sample pathloss data points. It represents the mean value of the pathloss samples in the scatter plot.

Random variations at a given distance around the regression line (i.e., mean value of the pathloss) occur for the following reasons: 1) when the tissue composition along the signal propagation path between the transmitter and receiver changes. This could be the case when different pairs of transmitter-receiver at different positions inside or on the abdomen have the same separation. This captures the random shadow and multipath fading caused by the body tissues. 2) when the relative orientations of capsule and/or the on-body antennas change with respect to each other. As discussed in earlier sections, due to the non-isotropic radiation pattern of the antennas, changes in their orientations could also impact the pathloss.
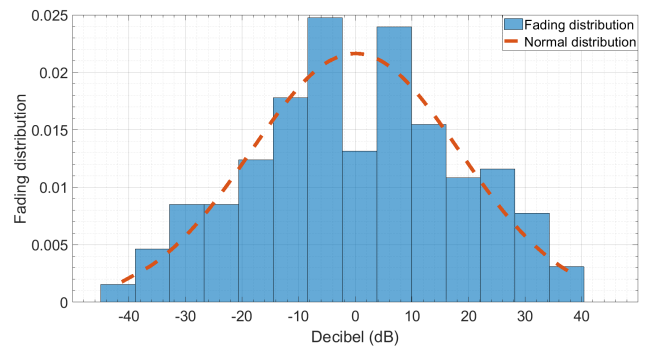
FIGURE 16. Fading distribution at 3.6 GHz.

Normalized histogram of this random variable at 3.6 GHz is shown in Fig. 16. As observed, a normal distribution with zero mean and standard deviation $\sigma_s(f)$ (i.e., $N(0, \sigma_s(f))$) fits the distribution of this random variable well and can be used to model the $S(f)$ component in the pathloss model (1). A Chi-Square Goodness-of-Fit test was used to confirm the Normal distribution.

Parameters of the pathloss model in (1) can be obtained through numerical analysis at any frequency $f \in$ [3.14.1] GHz. Variations of these parameters ($PL(d_0, f)$, $n(f)$, $\sigma_s(f)$) versus frequency are shown in Fig. 17. As observed, pathloss exponent $n(f)$ is nearly flat; however, the pathloss at reference distance and standard deviation $\sigma_s(f)$ is monotonically increasing with a slight slope. The mean value of these parameters ($\overline{PL}(d_0)$, $\bar{n}$, $\bar{\sigma}_s$) over the frequency range 3.1 GHz to 4.1 GHz are provided in Table 1.

The high pathloss exponent indicates the significant loss experienced by the UWB signal due to the human body tissues. Based on the maximum allowable transmit power and receiver sensitivity, this would limit the feasible range
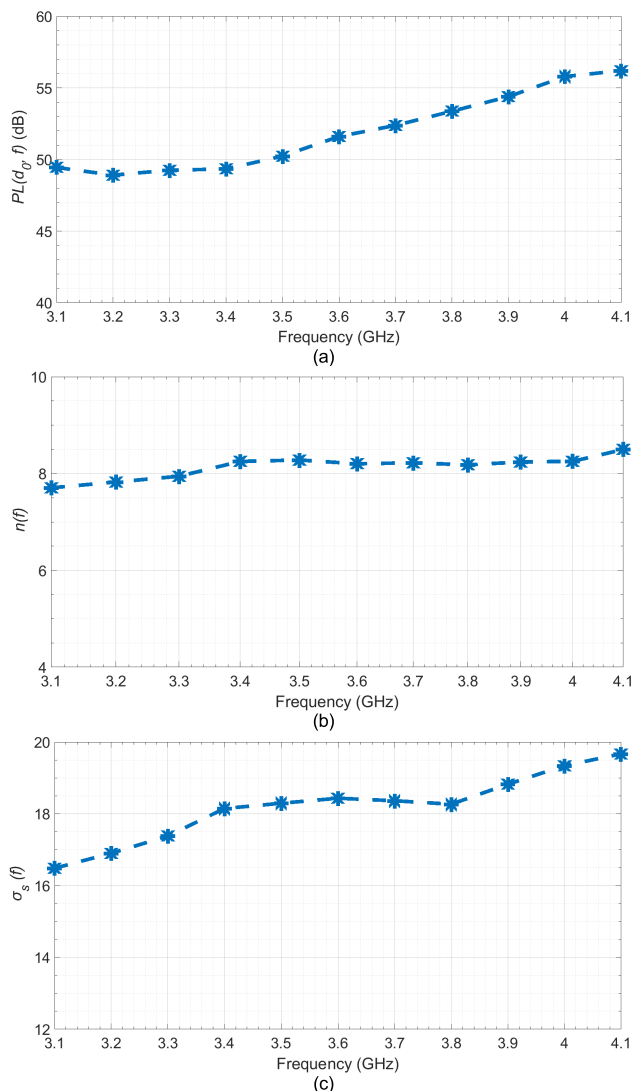
FIGURE 17. Parameters of the capsule pathloss model versus frequency: (a) PL (d_0, f), (b) n(f), (c) σ_S (f).

TABLE 1. Mean values of the parameters of the capsule pathloss model over 3.1 GHz to 4.1 GHz.

$\overline{PL}(d_0)$ (dB)	$\bar{n}$	$\overline{\sigma_S}$ (dB)
51.9	8.14	18.19

of communication with a capsule endoscope operating at UWB frequencies. Therefore, it can be expected that multiple receivers would be needed to exploit spatial diversity and achieve reliable communication with the capsule throughout its journey inside the small intestine. Our results also indicate the significant impact of the antenna orientation on the standard deviation of the fading component of the pathloss model. Due to the mobile nature of the capsule inside the small intestine, we believe that accurate modeling of the signal variations caused by the imperfect i.e., non-isotropic capsule antenna pattern is critical for a reliable communication with

a capsule endoscope. This necessitates better modeling of the fading component with realistic antennas, a more accurate computational body model and considering more pragmatic antenna positions for the measurements. These are all the intricate issues that we have considered in our study to generate the statistical pathloss model.
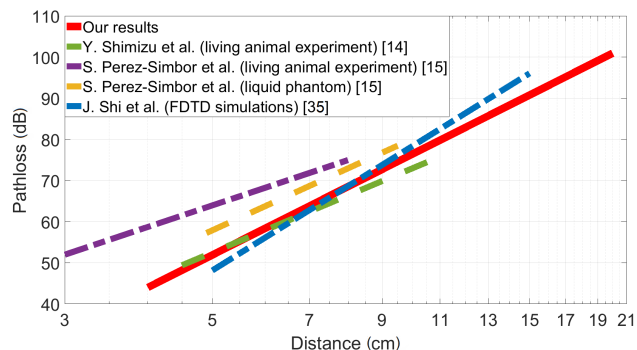

FIGURE 18. Comparison of the average pathloss.

Figure 18 shows the comparison of our results on the average pathloss versus distance with the results obtained by other researchers in [14], [15] and [35]. As observed, the pathloss exponent (i.e., $\bar{n}$) in our model is nearly in-line with the results obtained by other researchers. However, we believe that the fading component obtained in our research more accurately models the potential variations of the signal strength at the on-body receiver.

A. IMPLEMENTATION OF A LIQUID PHANTOM EXPERIMENT USING THE COMPUTATIONAL PLATFORM

To partially investigate the accuracy of the model obtained through virtual measurements using our computational platform, and comparison with the results through similar physical measurements, we emulated the liquid phantom measurement system described in [15, 30]. We developed a computational model of the multilayer container with identical dimensions, thickness, and material properties of each layer. This ensures identical propagation environments for comparison purposes. Since verified models of the UWB transmitter and receiver antennas in [15, 30] were not available, different antennas with approximately similar peak gain were used for the simulations, instead. For each transmitter antenna position on the grid inside the phantom and a given receiver position on the container surface, the channel pathloss for the frequencies 3.1 GHz to 4.1 GHz were computed using the computational platform. Statistical pathloss model for each frequency can be obtained following the methodology described earlier. Because of the non-identical antennas used in the physical and virtual measurements, a full comparison of the acquired pathloss models cannot be made. However, if the measurement positions for the antennas are carefully chosen, the pathloss exponent which is indicative of the rate at which the received signal strength decreases with distance is less impacted by the discrepancies in the antennas' performance. Figure 19 shows

the comparison of pathloss exponents for the frequency range 3.1 GHz to 4.1 GHz. As observed, the frequency dependent pathloss exponent obtained by the computational experiment closely matches the one obtained through the physical experiment.
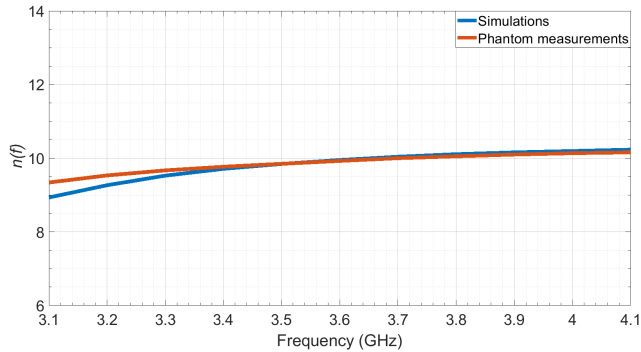

FIGURE 19. Comparison of the pathloss exponent $n(f)$ obtained through computational and physical experiments with a liquid phantom.

Other parameters of the pathloss model such as standard deviation of the $S(f)$ component in the pathloss model could not be compared as the gain pattern of the antennas used in simulations were not identical to the ones used in the physical experiments. A detailed study on the importance of the antenna position distribution on the accuracy of the resulting pathloss model can be found in [30].

VI. TIME DOMAIN ANALYSIS

Time domain characterization of UWB propagation channels in wireless implants and ingestible electronics is not an adequately explored topic in the literature. Authors in [32] and [33] have conducted preliminary time domain analysis and multipath study for an implant communication channel in the human chest. However, there are very few studies in the literature for capsule endoscopy application at UWB frequencies [34], [35]. In this section, based on the set of frequency responses collected for all the scenarios discussed earlier, we study the time domain response of the capsule channel and investigate the presence of multipath.

For a given capsule position, the time domain response of the channel is obtained by converting the frequency response using Inverse Fast Fourier Transform (IFFT). A modified Hann window is also used to reduce ringing and remove any discontinuity. Figure 20 shows an example of the time domain response for a capsule position that is 6 cm away from an on-body receiver. Hilbert Transform methodology has been used to detect the signal envelope (shown in red color). As observed, this channel can be approximately represented by a single pulse with a delay of about 1.5 ns. It is informative to understand the relationship between this delay and the line-of-sight distance between the transmitter and receiver. Normally, the propagation delay between a receiver-transmitter pair is equal to the distance between the pair
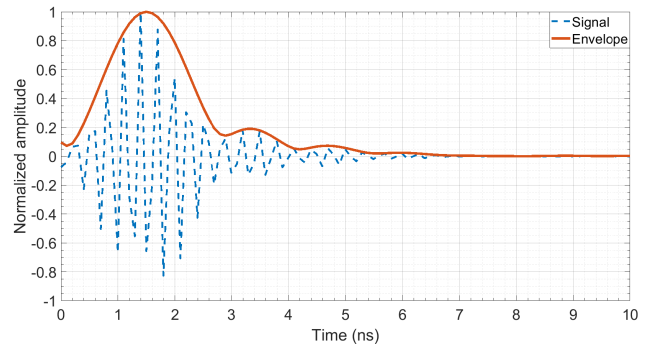

FIGURE 20. Time domain response of the channel (3.1 GHz to 4.1 GHz) between the capsule and an on-body receiver with a distance of 6 cm.

divided by the speed of the electromagnetics wave in free space (i.e., $c = 3 \times 10^8$ m/s). However, in the human body, the speed is affected by the dielectric properties of the tissues that the wave propagates through. Assume that ε_{avg} represents the average permittivity of the small intestine, muscle, fat, and skin over the frequency range 3.1 GHz to 4.1 GHz. Then, the average speed of the RF signal (v_{avg}) can be approximated by the following equation:

$$v_{avg} = \frac{c}{\sqrt{\varepsilon_{avg}}} \tag{2}$$

For capsule endoscopy application, $\varepsilon_{avg} = 49$; and therefore $v_{avg} = 42.86 \times 10^6$ m/s. Considering the 6 cm distance between the transmitter and receiver, the propagation delay of the channel is estimated to be $6 \times 10^{-2} / 42.86 \times 10^6 = 1.4$ ns. This delay reasonably matches the time associated with the peak amplitude of the time domain response as seen in Fig. 20.

Different dielectric properties of various tissues in the complex environment of the human body affect the propagation of RF waves transmitted from a wireless source inside the body. For implants or ingestible electronics, it is generally assumed that the human body environment is causing multipath. However, to the best of our knowledge, there are no reports that comprehensively indicate the presence or severity of multipath and its impact on the received signal. To investigate multipath in more detail, we obtained the time domain responses of all 200 channels discussed in Section V and looked for examples or scenarios where non-line-of-sight paths are observable in the time domain.

Since pulse width in the channel response is proportional to the inverse of the bandwidth, to be able to better distinguish multiple paths, we also considered higher bandwidth using the frequency range [3.1 to 5.1] GHz. For the frequency range 3.1 GHz to 4.1 GHz considered so far, two propagation paths would be easily distinguishable if they are separated by 2 ns or more. For 2 GHz bandwidth, this time reduces to 1 ns. Figure 21 shows the normalized amplitude of the time domain response for the example scenario discussed so far but using the frequency range 3.1 GHz to 5.1 GHz instead. No multipath behavior is observed for this channel even with
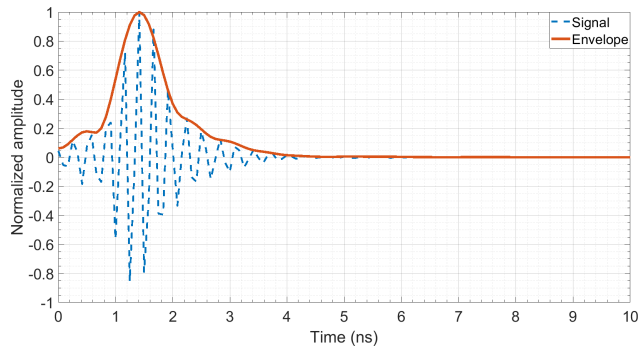
FIGURE 21. Time domain response of the channel (3.1 GHz to 5.1 GHz) between the capsule and an on-body receiver with a distance of 6 cm.

the higher bandwidth. Looking at most of the channels with the same capsule position but different on-body receivers also didn't bring up any visible multipath behavior.
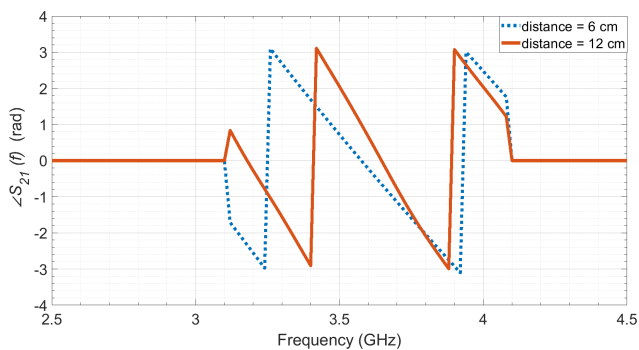

FIGURE 22. Comparison of $\angle S_{21}(f)$ for two channels between the capsule and two on-body receivers with distances = 6 cm and 12 cm.

The phase of the forward transmission coefficient of the channel (i.e., $\angle S_{21}(f)$) can also be used to investigate the impact of multipath. Figure 22 shows the phase of the $S_{21}(f)$ versus frequency for two separate on-body receivers at 6 cm and 12 cm distances from the capsule position. The linearity of the phase indicates that there is either one main propagation path (likely the line-of-sight) or other secondary paths are severely attenuated before reaching the receiver, and therefore cause very little or no phase distortion at the received signal. It is worth noting that, as expected, the slope in the phase plot at the receiver that is located 12 cm away from the capsule is almost double the slope for the channel with 6 cm distance.

The capsule position corresponding to figures 20, 21, and 22 is in the middle of the abdomen with no bone structure in its vicinity. Looking at other capsule positions inside the small intestine, we also selected a position in the lower segment of the abdomen, closer to the hip bone (i.e., the ilium which is the largest part of the pelvis). We calculated the channel response between this new position and an on-body receiver that is 14 cm away. Figure 23 shows the normalized amplitude of the time domain response for this channel using 3.1 GHz to 4.1 GHz as well as 3.1 GHz to 5.1 GHz frequency

ranges. The results indicate the existence of a strong second path for this capsule position.
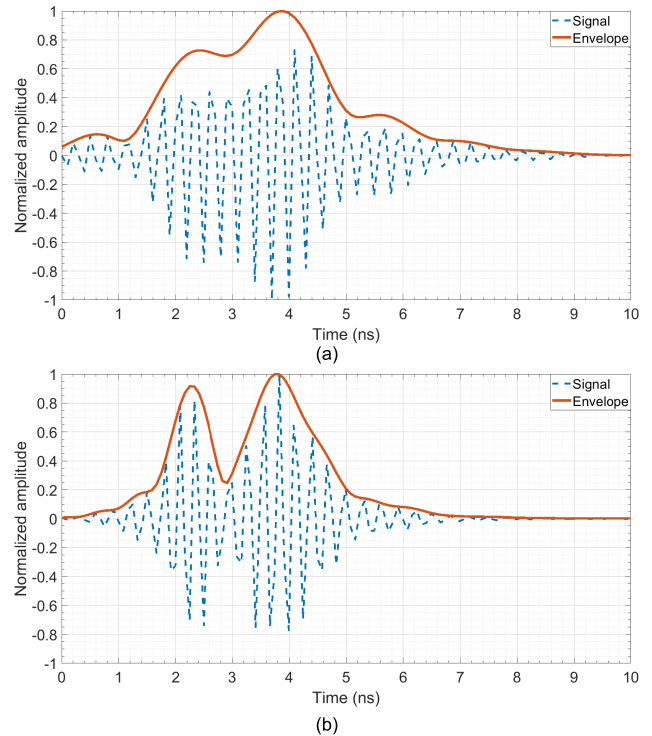

(a)

(b)

FIGURE 23. Time domain response of the channel between the capsule and an on-body receiver with a distance of 14 cm using (a) 3.1 GHz to 4.1 GHz (b) 3.1 GHz to 5.1 GHz.

Although it is conceivable that the bones could contribute to multipath fading of the received signal by causing reflection, refraction, or scattering, we also found evidence that they could lessen the impact of multipath by further shadowing (or blocking) a potential propagation path. For example, choosing a capsule position in the middle of the small intestine and an on-body receiver on the side of the abdomen, we conducted simulations to obtain the channel responses with and without the skeleton in the human body model. Figure 24 shows the results.

As observed, the broadening of the pulse after the removal of skeleton is indicative of interfering path(s) that would have otherwise been weakened by the bones in the vicinity of the signal propagation path. Comparing the amplitude and phase of the frequency response of this channel (i.e., $S_{21}(f)$) with and without the skeleton also points to the existence of multipath as seen in Figures 25 and 26. The fading in the amplitude of $S_{21}(f)$ around 3.3 GHz (Fig. 25) and the nonlinearity of the phase of $S_{21}(f)$ as evident in the phase derivative plot (Fig. 26(b)) are both indicative of the impact of multipath distortion in this channel.

In our investigation of the presence of multipath, we have observed scenarios where the first arrival path is not necessarily the direct path between the transmitter and receiver. There are possible capsule and receiver antenna
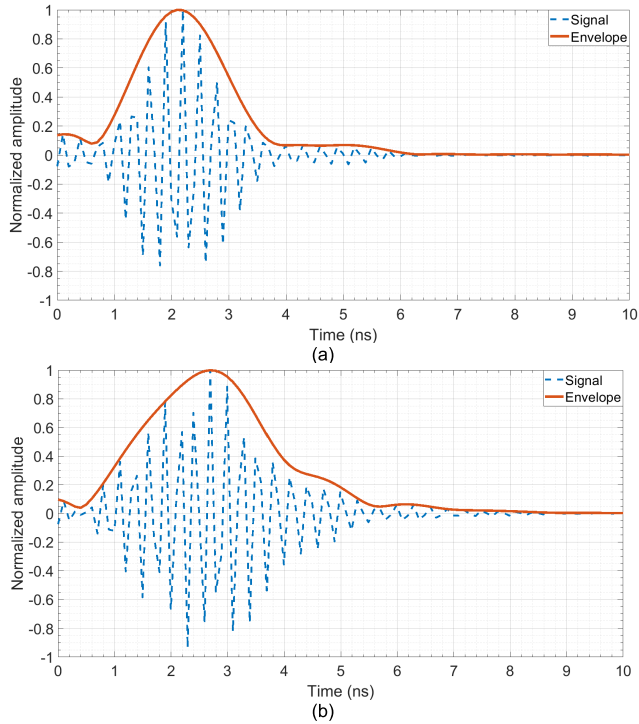
FIGURE 24. Time domain response of the channel between the capsule and an on-body receiver with a distance of 12 cm using the body model (a) with skeleton (b) without skeleton.
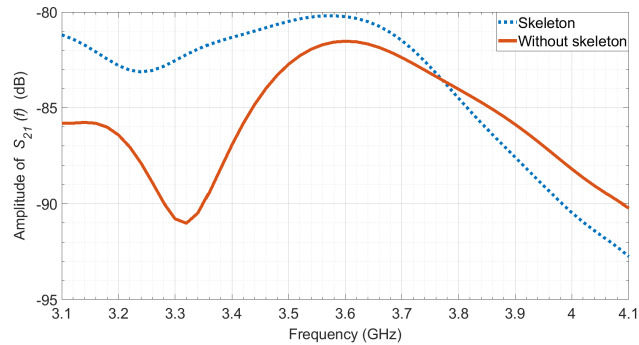

FIGURE 25. Amplitude of $S_{21}(f)$ for the channel between the capsule and an on-body receiver placed on the left side of the abdomen.

positions that could result in a first path being a diffracted path from the body surface (through creeping waves) while the weaker second path is the direct line-of-sight path between the transmitter-receiver pair. In those scenarios, the arrival time of the first component could be earlier that the arrival time of the direct line-of-sight path between the transmitter-receiver pair. This is again due to the higher speed of the electromagnetics wave on the body surface (for the diffracted path) versus in-body propagation speed (for the direct line-of-sight path).

Finally, our results in section VI indicates higher signal attenuation in the human body with increasing frequency. Therefore, it is informative to know the most effective range of the frequencies within the unlicensed UWB spectrum that can be used for capsule endoscopy. Consider $E(f_h)$ to
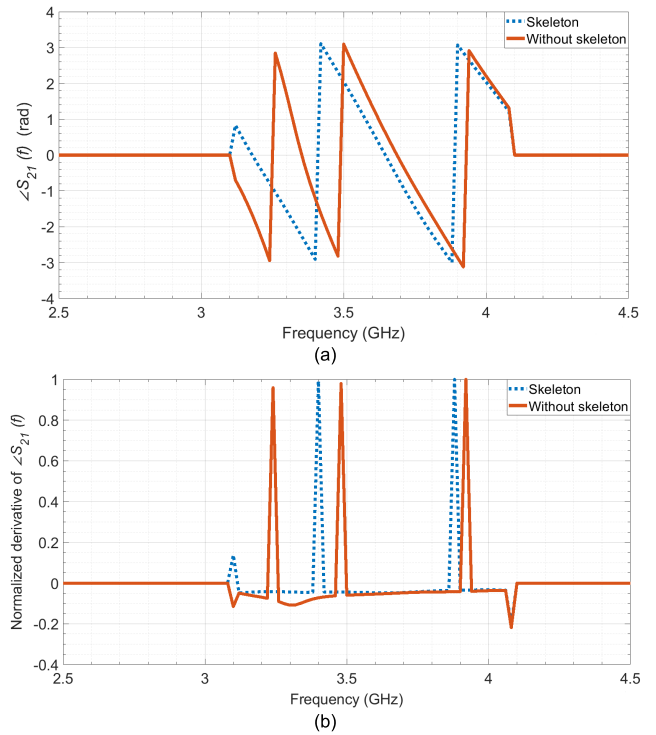

FIGURE 26. (a) $\angle S_{21}(f)$, (b) derivative of $\angle S_{21}(f)$ for the channel between the capsule and an on-body receiver on the abdomen side.

be the energy of the received signal when the bandwidth $f_h - 3.1$ GHz is utilized by the capsule UWB transmitter. Then, for a given transmitter and receiver locations, $E(f_h)$ can be calculated as follows.

$$E(f_h) = \int_{3.1 \times 10^9}^{f_h} |S_{21}(f)|^2 \, df \qquad (3)$$

Define the relative increase in the energy of the received signal when the bandwidth $f_h - 3.1$ GHz is utilized compared to the case when 3.1 GHz to 4.1 GHz frequency range is used by the following equation.

$$I(f_h) = \frac{E(f_h) - E(4.1)}{E(4.1)} \qquad (4)$$

For the examples discussed earlier in this section, $I(5.1) = 0.1245$, and $I(6.1) = 0.1349$. In other words, using 2 GHz or 3 GHz bandwidth only results in a 12% and 13% increase in the energy of the received signal respectively. For this reason, we conjecture that the practical range for using unlicensed UWB frequencies for capsule endoscopy application is 3.1 GHz to 4.1 GHz.

VII. CONCLUSION AND FUTURE WORK
An innovative 3D immersive system including a detailed computational human body and gastrointestinal tract models has been presented in this paper. The system allows for an in-depth study of the wireless propagation channel between a capsule endoscope and on-body receivers at UWB frequencies. A statistical pathloss model including a fading component that effectively captures the impact of

various body tissues as well as the antenna orientation for 3.1 GHz to 4.1 GHz frequency range has been developed. We have shown that this frequency range is more feasible for communication with a capsule endoscope within the unlicensed UWB spectrum. To the best of our knowledge, this is the first study that comprehensively captures the entire length of the small intestine while considering appropriate positions for capsule along its natural trajectory in order to conduct virtual measurements. To investigate the accuracy of the model obtained through virtual measurements using our computational platform, we also emulated a liquid phantom measurement system and observed that the frequency dependent pathloss exponent obtained by the computational experiment closely matches the one obtained through physical experiment. The ultimate verification of the pathloss model will require human subject experiments. As can be imagined, this is extremely challenging and involves developing a special hardware prototype and obtaining proper clinical approval.

The pathloss information presented in this paper can help with more accurate link budget and better understanding of the feasible communication range as the capsule traverses the small intestine. This knowledge can also assist in identifying the minimum number and optimal placements of the on-body receivers to ensure reliable signal reception from the capsule regardless of its position inside the GI tract. It is also conceivable to use array antennas and beamforming technology to achieve better signal strength, higher communication range or equivalently lower required transmit power by the capsule. Lower transmit power would translate to lower consumed energy which could help to alleviate the battery lifetime problem in capsule endoscopy applications. The authors are currently studying these problems and the results will be provided in future publications. The statistical pathloss model presented in this paper has been contributed to the IEEE 802.15 Task Group 6ma as part of the standard channel model for the capsule endoscopy use-case. IEEE 802.15.6ma is the revision of the standard IEEE 802.15.6-2012 for wireless body area networks.

Time domain analysis was also conducted to identify the presence of multipath for several capsule and on-body receiver positions. Due to the complexity and variety of the human body organs and tissues, it has been generally assumed that the UWB channel between a capsule endoscope or implant and an on-body receiver could exhibit strong multipath propagation. However, time domain channel responses examined in our study mostly revealed very few noticeable delayed paths (i.e., typically one line-of-sight and one non-line-of-sight paths). This is likely due to the very high attenuation experienced by longer propagation paths inside the human body. Therefore, we anticipate a tapped-delay-line channel model for capsule endoscopy at UWB frequencies would basically include two main components. More extensive studies are required to obtain the statistical distributions for the amplitude and delay of each component. The authors plan to continue this study and further characterize the time domain response of the UWB channel for capsule endoscopy.

REFERENCES

[1] A. F. Peery, S. D. Crockett, C. C. Murphy, E. T. Jensen, H. P. Kim, M. D. Egberg, J. L. Lund, A. M. Moon, V. Pate, E. L. Barnes, C. L. Schlusser, T. H. Baron, N. J. Shaheen, and R. S. Sandler, "Burden and cost of gastrointestinal, liver, and pancreatic diseases in the United States: Update 2021," *Gastroenterology*, vol. 162, no. 2, pp. 621–644, Feb. 2022, doi: 10.1053/j.gastro.2021.10.017.

[2] G. Iddan, G. Meron, A. Glukhovsky, and P. Swain, "Wireless capsule endoscopy," *Nature*, vol. 405, no. 6785, pp. 417–418, May 2000.

[3] M. Penazzio, "Small-bowel capsule endoscopy and device-assisted enteroscopy for diagnosis and treatment of small bowel disorders," *Eur. Soc. Gastrointestinal Endoscopy (ESGE) Clin. Guideline, Endoscopy*, vol. 47, pp. 352–376, Apr. 2015.

[4] G. J. Iddan and C. P. Swain, "History and development of capsule endoscopy," *Gastrointestinal Endoscopy Clinics North Amer.*, vol. 14, no. 1, pp. 1–9, Jan. 2004, doi: 10.1016/j.giec.2003.10.022.

[5] G. Ciuti, A. Menciassi, and P. Dario, "Capsule endoscopy: From current achievements to open challenges," *IEEE Rev. Biomed. Eng.*, vol. 4, pp. 59–72, 2011, doi: 10.1109/RBME.2011.2171182.

[6] M. R. Yuce and T. Dissanayake, "Easy-to-swallow wireless telemetry," *IEEE Microw. Mag.*, vol. 13, no. 6, pp. 90–101, Sep. 2012, doi: 10.1109/MMM.2012.2205833.

[7] C. Van de Bruaene, D. D. Looze, and P. Hindryckx, "Small bowel capsule endoscopy: Where are we after almost 15 years of use?" *World J. Gastrointestinal Endoscopy*, vol. 7, no. 1, pp. 13–36, Jan. 2015, doi: 10.4253/wjge.v7.i1.13.

[8] Z. Liao, R. Gao, C. Xu, and Z.-S. Li, "Indications and detection, completion, and retention rates of small-bowel capsule endoscopy: A systematic review," *Gastrointestinal Endoscopy*, vol. 71, no. 2, pp. 280–286, Feb. 2010, doi: 10.1016/j.gie.2009.09.031.

[9] *IEEE Standard for Local and Metropolitan Area Networks*, Standard IEEE 802.15.6-2012—Part 15.6, Wireless Body Area networks, 2012.

[10] K. Sayrafian-Pour, W.-B. Yang, J. Hagedorn, J. Terrill, and K. Y. Yazdandoost, "A statistical path loss model for medical implant communication channels," in *Proc. IEEE 20th Int. Symp. Pers., Indoor Mobile Radio Commun.*, Sep. 2009, pp. 2995–2999, doi: 10.1109/PIMRC.2009.5449869.

[11] J. Shi and J. Wang, "Channel characterization and diversity feasibility for in-body to on-body communication using low-band UWB signals," in *Proc. 3rd Int. Symp. Appl. Sci. Biomed. Commun. Technol. (ISABEL)*, Nov. 2010, pp. 1–4, doi: 10.1109/ISABEL.2010.5702784.

[12] D. Anzai, K. Katsu, R. Chavez-Santiago, Q. Wang, D. Plettemeier, J. Wang, and I. Balasingham, "Experimental evaluation of implant UWB-IR transmission with living animal for body area networks," *IEEE Trans. Microw. Theory Techn.*, vol. 62, no. 1, pp. 183–192, Jan. 2014, doi: 10.1109/TMTT.2013.2291542.

[13] K. M. S. Thotahewa, J.-M. Redoutè, and M. R. Yuce, "Propagation, power absorption, and temperature analysis of UWB wireless capsule endoscopy devices operating in the human body," *IEEE Trans. Microw. Theory Techn.*, vol. 63, no. 11, pp. 3823–3833, Nov. 2015, doi: 10.1109/TMTT.2015.2482492.

[14] Y. Shimizu, D. Anzai, R. Chavez-Santiago, P. A. Floor, I. Balasingham, and J. Wang, "Performance evaluation of an ultra-wideband transmit diversity in a living animal experiment," *IEEE Trans. Microw. Theory Techn.*, vol. 65, no. 7, pp. 2596–2606, Jul. 2017, doi: 10.1109/TMTT.2017.2669039.

[15] S. Perez-Simbor, C. Andreu, C. Garcia-Pardo, M. Frasson, and N. Cardona, "UWB path loss models for ingestible devices," *IEEE Trans. Antennas Propag.*, vol. 67, no. 8, pp. 5025–5034, Aug. 2019, doi: 10.1109/TAP.2019.2891717.

[16] M. Barbi, C. Garcia-Pardo, A. Nevárez, V. P. Beltrán, and N. Cardona, "UWB RSS-based localization for capsule endoscopy using a multilayer phantom and in vivo measurements," *IEEE Trans. Antennas Propag.*, vol. 67, no. 8, pp. 5035–5043, Aug. 2019, doi: 10.1109/TAP.2019.2916629.

[17] M. Särestöniemi, C. P. Raez, M. Berg, C. Kissi, M. Hämäläinen, and J. Iinatti, "WBAN radio channel characteristics between the endoscope capsule and on-body antenna," in *Body Area Networks: Smart IoT and Big Data for Intelligent Health Management*, vol. 297. Cham, Switzerland: Springer, 2019, pp. 360–373, doi: 10.1007/978-3-030-34833-5_27.

[18] M. Särestöniemi, C. Pomalaza-Ráez, C. Kissi, M. Berg, M. Hämäläinen, and J. Iinatti, "WBAN channel characteristics between capsule endoscope and receiving directive UWB on-body antennas," *IEEE Access*, vol. 8, pp. 55953–55968, 2020, doi: 10.1109/ACCESS.2020.2982247.

[19] M. Särestöniemi, A. Taparugssanagorn, J. Wisanmongkol, M. Hämäläinen, and J. Iinatti, "Comprehensive analysis of wireless capsule endoscopy radio channel characteristics using anatomically realistic gastrointestinal simulation model," *IEEE Access*, vol. 11, pp. 35649–35669, 2023, doi: 10.1109/ACCESS.2023.3263555.

[20] M. Särestöniemi, C. Pomalaza-Raez, and J. Iinatti, "Radio channel study for colon capsule endoscopy with low-band UWB multiple antenna system," in *Proc. IEEE 16th Int. Symp. Med. Inf. Commun. Technol. (ISMICT)*, May 2022, pp. 1–6, doi: 10.1109/ISMICT56646.2022.9828189.

[21] C. Garcia-Pardo, A. Fornes-Leal, M. Frasson, V. Pons-Beltrán, and N. Cardona, "Effect of breathing on UWB propagation characteristics for ingestible and implantable devices," *IEEE Trans. Antennas Propag.*, vol. 70, no. 4, pp. 3118–3122, Apr. 2022, doi: 10.1109/TAP.2021.3118724.

[22] S. L. Cotton, R. D'Errico, and C. Oestges, "A review of radio channel models for body centric communications," *Radio Sci.*, vol. 49, no. 6, pp. 371–388, Jun. 2014, doi: 10.1002/2013RS005319.

[23] K. Y. Yazdandoost and K. Sayrafian, *Channel Model for Body Area Network*, Standard IEEE P802.15-08-0780-12, P802.15 Work. Group for Wireless Personal Area Networks, Apr. 2009.

[24] K. Sayrafian-Pour, J. Hagedorn, W.-B. Yang, and J. Terrill, "A virtual reality platform to study RF propagation in body area networks," in *Proc. IEEE 3rd Int. Conf. Cognit. Infocommunications (CogInfoCom)*, Dec. 2012, pp. 709–713, doi: 10.1109/CogInfoCom.2012.6421944.

[25] M. Hanscom and D. R. Cave, "Endoscopic capsule robot-based diagnosis, navigation and localization in the gastrointestinal tract," *Frontiers Robot. AI*, vol. 9, Sep. 2022, Art. no. 896028, doi: 10.3389/frobt.2022.896028.

[26] K. Y. Yazdandoost, "Antenna for wireless capsule endoscopy at ultra wideband frequency," in *Proc. IEEE 27th Annu. Int. Symp. Pers., Indoor, Mobile Radio Commun. (PIMRC)*, Sep. 2016, pp. 1–5, doi: 10.1109/PIMRC.2016.7794781.

[27] K. Y. Yazdandoost and R. Kohno, "UWB antenna for wireless body area network," in *Proc. Asia–Pacific Microw. Conf.*, Dec. 2006, pp. 1647–1652, doi: 10.1109/APMC.2006.4429724.

[28] K. Y. Yazdandoost and R. Kohno, "Ultra wideband L-loop antenna," in *Proc. IEEE Int. Conf. Ultra-Wideband*, Sep. 2005, pp. 201–205, doi: 10.1109/ICU.2005.1569984.

[29] (Mar. 2013). *Given Imaging-PillCam Capsule Endoscopy User Manual, RAPID v8.0*. [Online]. Available: http://www.medtronic.com/content/dam/covidien/library/us/en/product/diagnostic-testing/pillcam-rapid-v8-user-manual.pdf

[30] S. Perez-Simbor, K. Krhac, C. Garcia-Pardo, K. Sayrafian, D. Simunic, and N. Cardona, "Impact of measurement points distribution on the parameters of UWB implant channel model," in *Proc. IEEE Conf. Standards Commun. Netw. (CSCN)*, Oct. 2018, pp. 1–6, doi: 10.1109/CSCN.2018.8581808.

[31] H. Tangelder and A. Fabri. (2019). *dD Spatial Searching*. CGAL User and Reference Manual. CGAL Editorial Board. [Online]. Available: https://doc.cgal.org/latest/Spatial_searching/index.html

[32] A. Khaleghi, R. Chávez-Santiago, and I. Balasingham, "Ultra-wideband statistical propagation channel model for implant sensors in the human chest," *IET Microw., Antennas Propag.*, vol. 5, no. 15, p. 1805, 2011.

[33] J. Wang and Q. Wang, "Channel modeling and BER performance of an implant UWB body area link," in *Proc. 2nd Int. Symp. Appl. Sci. Biomed. Commun. Technol.*, Nov. 2009, pp. 1–4.

[34] S. Perez-Simbor, C. Garcia-Pardo, and N. Cardona, "Initial delay domain UWB channel characterization for in-body area networks," in *Proc. 13th Int. Symp. Med. Inf. Commun. Technol. (ISMICT)*, May 2019, pp. 1–5, doi: 10.1109/ISMICT.2019.8743767.

[35] J. Shi, D. Anzai, and J. Wang, "Channel modeling and performance analysis of diversity reception for implant UWB wireless link," *IEICE Trans. Commun.*, vol. E95.B, no. 10, pp. 3197–3205, 2012.

KATJANA LADIC received the B.Sc. degree in electrical engineering and information technology and the M.Sc. degree in information and communication technology from the Faculty of Electrical Engineering and Computing (FER), University of Zagreb, Zagreb, Croatia, in 2014 and 2016, respectively. She is currently pursuing the Ph.D. degree with the University of Zagreb. She is a Research Associate with the Information Technology Laboratory (ITL), National Institute of Standards and Technology (NIST), Gaithersburg, MD, USA. Her research interests include the analysis and modeling of wireless communication channels for wearables and implants. She was a recipient of the IEEE CSCN 2018 Best Paper Award and the NIST ITL Outstanding Conference Paper Awards, in 2019 and 2022.

KAMRAN SAYRAFIAN (Senior Member, IEEE) received the M.S. degree in electrical and computer engineering from Villanova University and the Ph.D. degree in electrical and computer engineering from the University of Maryland.

He is currently a Senior Scientist at the Information Technology Laboratory of the National Institute of Standards and Technology (NIST), Gaithersburg, ML, USA, where he leads a strategic program related to the application of the Internet of Things (IoT) in healthcare. He is also an affiliate Associate Professor of Concordia University in Montreal, Canada, since 2016 and the Co-Chair of the Vertical Track on Health and Well-Being at the COST CA20120 "Intelligence-Enabling Radio Communications for Seamless Inclusive Interactions". Prior to joining NIST, he was the Co-Founder of Zagros Networks, Inc. a fabless semiconductor company based in Rockville, ML, USA, where he served as the President and Senior Member of the architecture team. He has served as the Technical Program Committee and Executive Co-Chair of the IEEE PIMRC 2014 and organizer of several other IEEE ComSoc Conferences and international workshops focused on the applications of wireless communication in healthcare. He was also a member of the Editorial Board of the IEEE *Wireless Communication Magazine* from 2016 to 2020. His current research interests include body area networks, micro energy harvesting, automatic exposure notification, and IoT technology in healthcare. He has published over 120 conference and journal papers, and book chapters, and has been the recipient of the IEEE PIMRC 2009, SENSORCOMM 2011, IEEE CSCN 2018 and IEEE EuCNC 2019 best paper awards. He was a major contributor to the development of the IEEE802.15.6 international standard on Body Area Networks; and the recipient of the 2015 U.S. Department of Commerce Bronze Medal for his contribution to this emerging field. In 2014, he also served as the U.S. Embassy Science Fellow in Croatia. He is the co-inventor/inventor of four U.S. patents and a Fellow of the Washington Academy of Sciences.

DINA ŠIMUNIĆ (Senior Member, IEEE) received the B.Sc. and M.Sc. degrees in electrical engineering from the Faculty of Electrical Engineering and Computing (FER), University of Zagreb, Zagreb, Croatia, in 1985 and 1992, respectively, and the Dr.Sc. degree from the Graz University of Technology, Austria, in 1995.

Since 1991, she has been with the Department for Wireless Communications, Faculty of Electrical Engineering, University of Zagreb. She was a Guest Professor with research laboratories Wandel and Goltermann, Germany, and Motorola Inc., USA, in 1996. In 2007, she was promoted to Full Professor. She is currently the Leader of the group strategy towards the development of materials for education about standardization and identification of common requirements with ITU. She is the Leader of the Scientific Green Engineering Laboratory (GEL). She participated in five and led three scientific projects of the Croatian Ministry of Science, Education and Sports. She was a WP Coordinator of the EU FP7 Project: eWALL. She was a Collaborator in the research project, financed through structural funds of the EU and the Ministry of Science, Education and Sports: "ICTGEN" (Information and Communication Technology for Generic and Energy-efficient Solutions with Application in e-/m-Health). She published more than 100 papers in journals and conference proceedings in the field of secure routing protocols against denial-of-service attacks in mobile ad hoc networks, cognitive radio systems, radiofrequency simulations, and biomedical effects of electromagnetic fields.

Prof. Šimunić participated in ten international program committees of scientific conferences. She serves as a member of the editorial board for the international scientific journal *Journal of Structural Engineering* and a Reviewer of *Wireless Personal Communications* and many other international scientific journals. In the European Commission, she acted as the Vice-Chair of COST, for precompetitive research in information and communication technologies. She served as the Editor-in-Chief for the *Journal of Green Engineering*. She was the Vice-President of the Telecommunications Council, Croatia. She is also the President of the Technical Committee for Telecommunications, Croatian Standards Institute.

KAMYA YEKEH YAZDANDOOST (Senior Member, IEEE) was a Senior Researcher with the National Institute of Information and Communications Technology (NICT), Japan, from 2003 to 2016. He was a Finland Distinguished Professor Program (FiDiPro) Fellow with the Centre for Wireless Communications (CWC), University of Oulu, Finland, from 2010 to 2015. He was a fellow with the Department of Electrical Engineering and Automation, Aalto University, Finland, from 2017 to 2020. He was with the Technology Engineering Group, International Iberian Nanotechnology Laboratory (INL), Portugal, from 2020 to 2021. He is currently with the Optical Access Network Laboratory, KDDI Research Inc., Fujimino, Saitama, Japan. He is also an Adjunct Professor with CWC, Department of Communications Engineering, University of Oulu. He is the coauthor of the book *Wireless Body Area Networks* and contributed to more than 160 refereed journal articles and conference papers, technical documents, and book chapters. He holds seven patents. His research interests include antenna design, RF and electromagnetic waves, 5G, body area networks, wireless communications, and RF energy harvesting. He is a Life Member of the IEEE Microwave Theory and Technology Society (formerly the IEEE Microwave Theory and Techniques Society). He was a Representative and a Contributing Member of the NICT, European Cooperation in Science and Technology, COST2100 Action, and COST-IC1004 Action, and chairing the Body Environment Group of this Action for four years. He was a recipient of the Best Paper Award of the IEEE PIMRC 2009 and the IEEE ISMICT 2014 Conferences. He was a recipient of the Extra Ordinary Achievements Medal from NICT, in 2013. He was the IEEE Chair of the Committee for channel modeling of wireless body area network standardization and the Co-Editor of the channel modeling documents of the IEEE.802.15.6 on WBAN Standardization. He was a guest editor of several international journals. He served in various positions as the workshop chair, the track chair, a session organizer, a steering committee member, and a technical committee member for over 70 international conferences.

• • •